

---

# A Hybrid Meshless/Spectral-Element Method for the Shallow Water Equations on the Sphere

Christopher D. Blakely

*Center for Scientific Computation and Mathematical Modeling, University of Maryland, College Park, MD 20742-3289, U.S.A.; E-mail: cblakely@cscamm.umd.edu, www.cscamm.umd.edu/~cblakely*

**Abstract.** A hybrid approximation scheme for the shallow-water equations on the sphere is proposed which utilizes spectral-element approximation coupled with regional meshless collocation. The issue of satisfying continuity conditions across spectral-element to meshless collocation interfaces for this domain decomposition method is discussed and gives an example of a meshless collocation framework which can be successfully coupled with spectral-element approximation. We conclude the paper with numerical examples using the proposed hybrid scheme on two well-known standardized test problems for the rotational shallow-water equations on the sphere.

**Key words:** Meshless methods, spectral-element approximation, shallow-water equations.

## 1 Introduction and Motivations

The purpose of this paper will focus on constructing an innovative hybrid approximation method for geophysical fluid dynamics. To accomplish such a task, we will focus on the shallow-water equations which provide a useful model to global climate modeling because their solutions include nonlinear effects and wave structures similar to those of the full primitive equations of the atmosphere. The main backbone of this hybrid meshless/spectral-element shallow-water model will be focusing on incorporating a unique regional scale approximation method. This regional scale method will be accomplished by using a robust meshless approximation scheme called the empirical Backus-Gilbert reproducing kernel developed by Blakely in [5]. The advantage of such a hybrid approximation is two-fold: (1) high-order approximation results can be obtained in complex shaped geometries without the need of a mesh. Thus, no remeshing of a local region into smaller rectangles is needed, ultimately speeding up the computation time; (2) the Backus-Gilbert reproducing kernel method has been shown to be endowed with the unique power of ignoring oscillatory effects

in scattered data. This will be useful when the spectral approximation forms high oscillations due to discontinuities in the data.

This article is organized as follows. Section 2 begins with a brief review of the shallow-water equations defined on the cubed-sphere and its discretization in time using a semi-implicit time stepping scheme. We follow this discussion in Section 3 with a brief review of the spectral-element and Backus-Gilbert reproducing kernel discretization methods of the time-discrete shallow-water equations. Next, we present the three-field variational formulation which effectively couples the two types of approximations in a weak sense by introducing two additional approximation spaces on the interfaces between the approximation, akin to domain decomposition and the mortar element method. Implementation of the coupling is then given and then finally, in order to verify the mathematical correctness of the algorithms presented in this paper and to validate the performance hybrid model, we conclude the paper with some standardized test cases which were proposed by Williamson et al. in [22].

## 2 The Shallow-Water Equations on the Cubed-Sphere

Being the simplest form of motion equations that can approximate the horizontal structure of the atmosphere or the dynamics of oceans, the shallow-water equations have been used as a robust testing model in atmospheric and oceanic sciences. The solutions can represent certain types of motion including Rossby waves and inertia-gravity waves while describing an incompressible fluid subject to gravitational and rotating acceleration. The governing equations for the inviscid flow of a thin layer of fluid in 2-D are the horizontal momentum and continuity equations for the velocity  $\mathbf{u} = (u_1, u_2)$  and the geopotential height  $\eta$ .

While there are many different ways of defining the shallow-water equations, we focus in this model on cubed-sphere geometry originally proposed by Sadourny in [17] and used in other global models in recent years such as [20] and [21]. We begin by a brief review of the cubed-sphere while adopting notational conventions from [20]. Consider a cube inscribed inside a sphere where each corner of the cube is a point in the sphere and where each face of the cube is subdivided into  $N_E$  subregions. The goal is to project each face of the cube onto the sphere and in effect, obtain a quasi-uniform spherical grid of  $6 \times N_E$  subregions which can be further subdivided into many spectral element and meshless collocation subregions. In the mapping of the cube to sphere, each face of the cube is constructed with a local coordinate system and employs metric terms for transforming between the cube and the sphere which will now be defined.

Let  $(\alpha, \beta)$  be equal angular coordinates such that  $-\pi/4 \leq \alpha, \beta \leq \pi/4$ . Then any  $x_1$  and  $x_2$  on a face  $P_i$  of the cube is related through  $x_1 = \tan \alpha, x_2 = \tan \beta$ . We denote  $\mathbf{r}$  the corresponding position vector on the sphere with longitude  $\lambda$  and

latitude  $\theta$ . For such an equiangular projection, we define basis vectors  $\mathbf{a}_1 = \mathbf{r}_\alpha$  and  $\mathbf{a}_2 = \mathbf{r}_\beta$  which may be written as

$$\mathbf{r}_\alpha = \frac{1}{\cos^2 \alpha} \mathbf{r}_{x_1}, \quad \mathbf{r}_\beta = \frac{1}{\cos^2 \beta} \mathbf{r}_{x_2}, \quad (1)$$

where  $\mathbf{r}_{x_1}$  and  $\mathbf{r}_{x_2}$  are defined as  $\mathbf{r}_{x_1} = (\cos \theta \lambda_{x_1}, \theta_{x_1})$  and  $\mathbf{r}_{x_2} = (\cos \theta \lambda_{x_2}, \theta_{x_2})$ . The metric tensor  $g_{ij}$ ,  $i, j \in [1, 2]$  can be derived as

$$g_{ij} = \mathbf{a}_i \cdot \mathbf{a}_j = \frac{1}{r^4 \cos^2 \alpha \cos^2 \beta} \begin{bmatrix} 1 + \tan^2 \alpha & -\tan \alpha \tan \beta \\ -\tan \alpha \tan \beta & 1 + \tan^2 \beta \end{bmatrix},$$

where  $r^2 = 1 + \tan^2 \alpha + \tan^2 \beta$  and the Jacobian of the transformation and the matrix  $\tilde{\mathbf{A}}$  are, respectively,

$$\sqrt{g} = [\det(g_{ij})]^{1/2} = \frac{1}{r^3 \cos^2 \alpha \cos^2 \beta}, \quad \tilde{\mathbf{A}} = \begin{bmatrix} \cos \theta \lambda_\alpha & \cos \theta \lambda_\alpha \\ \theta_\alpha & \theta_\beta \end{bmatrix}.$$

While using the definition of  $g_{ij}$  given in (2), we can write transformations between covariant and contravariant components of a vector  $\mathbf{v}$  as

$$\begin{bmatrix} u_2 \\ u_2 \end{bmatrix} = \begin{bmatrix} g_{11} & g_{12} \\ g_{21} & g_{22} \end{bmatrix} \begin{bmatrix} u^1 \\ u^2 \end{bmatrix}, \quad \begin{bmatrix} u^1 \\ u^2 \end{bmatrix} = \begin{bmatrix} g^{11} & g^{12} \\ g^{21} & g^{22} \end{bmatrix} \begin{bmatrix} u_1 \\ u_2 \end{bmatrix}. \quad (2)$$

With the metric terms defined, we can now write the shallow water equations in the curvilinear coordinates system to be integrated on the cubed-sphere. In such a coordinate system, the shallow-water equations can be written as follows

$$\begin{aligned} \frac{\partial u^i}{\partial t} &= -g^{ij} \left[ \epsilon_{jkl} u^k g(f + \zeta) + \frac{\partial}{\partial x^j} \left( \frac{1}{2} u_k u^k \right) + \frac{\partial \eta}{\partial x^j} \right], \\ \frac{\partial \eta'}{\partial t} &= -u^j \frac{\partial \eta}{\partial x^j} - \frac{\eta}{g} \frac{\partial}{\partial x^j} (g u^j). \end{aligned}$$

Here, we define  $\eta = \eta' + \eta_0$ ,  $f$  is the Coriolis force and  $\zeta$  is the relative vorticity. Covariant and contravariant vectors are defined through the short-hand metric tensor notation  $u^i = g^{ij} u_j$ ,  $g^{ij} = (g_{ij})^{-1}$ . Furthermore, using  $\epsilon_{ij}$  as the two-dimensional permutation matrix, the divergence and relative vorticity can be calculated as

$$g \nabla \cdot \mathbf{v} = \frac{\partial}{\partial x^j} (g u^j), \quad g \zeta = \epsilon_{ij} \frac{\partial u_j}{\partial x^i}. \quad (3)$$

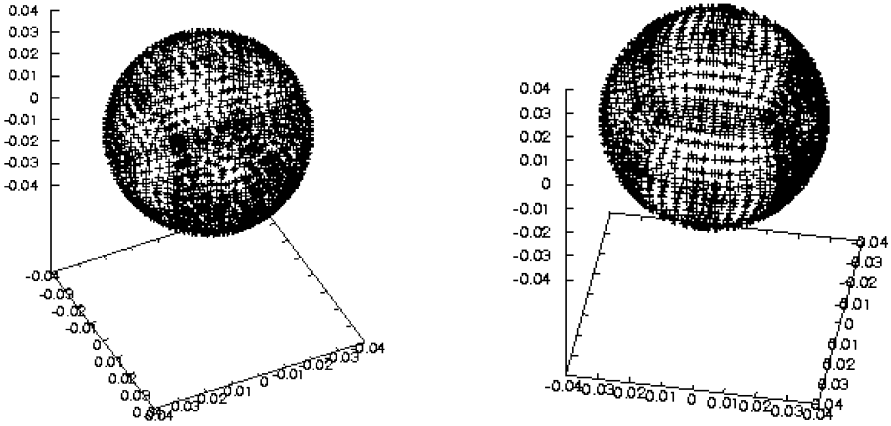


Fig. 1. Hybrid cube.

We note that the metric terms can be precalculated and stored once the issue of discretizing the cube has been resolved. To this end, we discuss the discretization of the cubed-sphere using the spectral element method in Section 3.1 and the meshless collocation method in Section 3.2. An example of the resulting discretized cube is shown in Figure 1.

### 2.1 Semi-Implicit Time Discretization

As an integral part of the hybrid meshless/spectral-element model, the semi-implicit time stepping scheme which we discuss in this subsection has many computational advantages. Semi-implicit time-stepping schemes were first used in atmospheric models in order to alleviate the problem of stability constraints ultimately due to the fast moving gravity waves in the discrete shallow water equations [20]. They have been successfully applied for allowing an increase in the time step without affecting the atmospherically important Rossby waves. Such a semi-implicit method is described in this subsection and was originally proposed in the spectral element model developed in [20].

In the hybrid meshless/spectral-element method, the semi-implicit time stepping is composed of an explicit leapfrog scheme for the advection terms combined with a Crank–Nicholson scheme for the gradient and divergence terms. Adopting the difference notation  $\delta u^i = u^{i(n+1)} - u^{i(n-1)}$  and  $\delta \eta^i = \eta^{(n+1)} - \eta^{(n-1)}$ , the time discretized shallow water equations in curvilinear coordinates can be written as

$$\begin{aligned} \delta u^i + \Delta t g^{ij} \frac{\partial}{\partial x^j} (\delta \eta) &= 2\Delta t \left[ -g^{ij} \frac{\partial}{\partial x^j} (\eta)^{n-1} + f_u^{i(n)} \right], \\ \delta \eta^i + \Delta t \frac{\eta_0}{g} \frac{\partial}{\partial x^j} (g \delta u^j) &= 2\Delta t \left[ \frac{\eta_0}{g} \frac{\partial}{\partial x^j} (g u^j)^{n-1} + f_\eta^{i(n)} \right], \end{aligned}$$

where the tendencies  $f_u$  and  $f_\eta$  contain nonlinear terms along with the Coriolis term, namely

$$f_u = -g^{ij} \left[ \epsilon_{jkl} u^{k(n)} g (f + \zeta^n) + \frac{\partial}{\partial x^j} \left( \frac{1}{2} u_k u^k \right)^n \right],$$

and

$$f_\eta = -u^j \frac{\partial \eta}{\partial x^j}.$$

Lastly, bringing the implicit terms to the left hand side of the equation and the explicit terms to the right, we end up with the time discrete evolution form of the shallow water equations

$$u^{i(n+1)} + \Delta t g^{ij} \frac{\partial}{\partial x^j} (\eta)^{n+1} = u^{i(n-1)} - \Delta t g^{ij} \frac{\partial}{\partial x^j} (\eta)^{n-1} + 2\Delta t f_u^{i(n)} \quad (4)$$

$$\eta^{n+1} + \Delta t \frac{\eta_0}{g} \frac{\partial}{\partial x^j} (g u^j)^{n+1} = \eta^{n-1} - \Delta t \frac{\eta_0}{g} \frac{\partial}{\partial x^j} (g u^j)^{n-1} + 2\Delta t f_\eta^n \quad (5)$$

which is now in the form needed for spatial discretization using the hybrid meshless/spectral-element. Because of the Crank–Nicholson terms, the storage of two previous time steps is needed. The overall performance of this semi-implicit method is reduced to the performance of a robust solver that can ultimately be parallelizable in an efficient manner for obtaining the solution at the  $n + 1$  time step. The preconditioned conjugate gradient method using a block-jacobi type preconditioner offers such an approach but at the cost of inter-elemental communication at every iteration step of the iterative solver. The method is of course highly dependent on the spatial approximation scheme and will be discussed in the next two subsections. To this end, we first briefly review the construction of the nodal spectral element approximation on the cubed-sphere.

### 3 Hybrid Meshless/Spectral-Element Discretization

#### 3.1 Spectral-Element Discretization

The spectral element formulation for the cubed sphere begins by decomposing each face on the unit cube denoted by  $P_i$ ,  $i = 1, \dots, 6$  into  $N_e$  nonoverlapping subdomain elements  $\Omega^e$  of equal area which are each referenced to a standard element  $\Omega_{st} = [-1, 1]^2$  by a mapping  $\mathbf{x}^e(r, s) \in \Omega^e$  for  $(r, s) \in \Omega_{st}$ . The mapping also has a well defined inverse  $(r, s)^e(\mathbf{x}) \in \Omega_{st}$ ,  $\mathbf{x} \in \Omega^e$ . Since two fields are being approximated in

the discrete shallow water equations, namely the velocity and the geopotential, two different approximation spaces are needed. As in most shallow water models, we adapt the so-called staggered grid approach to discretization. We begin by defining the approximation space for the velocity as  $V_N := \mathbb{P}_{N,N_e} \cap H^1(P_i)$ , where  $\mathbb{P}_{N,N_e}$  is the space of piecewise continuous functions that map to polynomials of degree less than or equal  $N$  to the reference element on face  $i$ . Namely,

$$\mathbb{P}_{N,N_e}(P_i) := v(\mathbf{x}^e(r, s))|_{\Omega^e} \in \mathbb{P}_N(r) \otimes \mathbb{P}_N(s), \quad e = 1, \dots, N_e,$$

where  $\mathbb{P}_N(r)$  is the space of all polynomials of degree less than or equal to  $N$ . In order to facilitate inter-element continuity on  $\Omega^e$  for all  $e \in [1, N_e]$  and more globally, inter-face continuity on  $P_i$ ,  $i = 1, \dots, 6$ , nodal Lagrangian interpolants are used to construct the basis within each element. In this paper, we use Lagrangian interpolants constructed from orthogonal Legendre functions of degree  $p$ .

While many spectral-element and spectral collocation models of fluid dynamics such as the ones found in [19] have utilized a staggered grid where the pressure/geopotential field on each element is discretized on an  $N - 2$  Gauss–Legendre distribution which does not include the boundaries of the element, this hybrid meshless/spectral-element model relies on boundary information of the geopotential field as explained in the next section on the three-field formulation for the shallow water equations. We thus build a staggered grid for the geopotential field which includes the boundaries of each element  $\Omega^e$  by considering the space  $M_N := \mathbb{P}_{(N-2,N_e)} \cap L^2(P_i)$  and distributing  $(N - 2)^2$  Gauss–Lobatto–Legendre points  $(\xi_i^1, \xi_j^2)$ .

Using the space  $M_N$ , the geopotential is expanded in a similar manner to the velocity components by using the  $(N - 2)$ -th degree Lagrangian interpolants  $\tilde{\pi}_i$  as

$$\eta(r, s)|_{\Omega^e} = \sum_{i=0}^{N-2} \sum_{j=0}^{N-2} \eta_{ij}^e \tilde{\pi}_i(r) \tilde{\pi}_j(s),$$

with  $\eta_{ij}^e$  being the nodal values of the geopotential at  $(\xi_i^1, \xi_j^2)$ . This expansion will require evaluation not only on the geopotential grid, but on the velocity grid as well. As will be shown later, the geopotential field provides the means for coupling the spectral element and meshless collocation approximations.

With the definitions of the Lagrangian nodal expansion and quadrature rule in place for each element, we can now apply weak formulation to the semi-implicit time discretized shallow water equations. Find  $(u^i, \eta) \in V_N \times M_N$  such that for all  $(v_i, q) \in V_N \times M_N$

$$\begin{aligned}
 & \langle \mathbf{u}^{i(n+1)}, v_i \rangle - \Delta t g^{ij} \left\langle \eta^{n+1}, \frac{\partial}{\partial x^j} v_i \right\rangle \\
 &= \langle \mathbf{u}^{i(n-1)}, v_i \rangle + \Delta t g^{ij} \left\langle \eta^{n-1}, \frac{\partial}{\partial x^j} v_i \right\rangle + 2\Delta t \langle f_u^{i(n)}, v_i \rangle, \\
 & \langle \eta^{n+1}, q \rangle + \Delta t \frac{\eta_0}{g} \left\langle q, \frac{\partial}{\partial x^j} (g u^j)^{n+1} \right\rangle \\
 &= \langle \eta^{n-1}, q \rangle - \Delta t \frac{\eta_0}{g} \left\langle q, \frac{\partial}{\partial x^j} (g u^j)^{n+1} \right\rangle + 2\Delta t \langle f_\eta^n, q \rangle. \tag{6}
 \end{aligned}$$

With the matrices, cubed-sphere metrics, and Coriolis forcing constructed on each element, the semi-implicit scheme can now be formulated into  $N_e$  local Helmholtz problems where the geopotential is solved at every timestep from a discrete Helmholtz problem and then ‘communicated’ to the velocity field. Writing the assembled discrete shallow water system from the previous subsection in matrix-vector form, we get

$$\begin{bmatrix} \mathbf{B}^t & -\mathbf{D}^t \\ \mathbf{D}^t & \tilde{\mathbf{B}}^t \end{bmatrix} \begin{bmatrix} \mathbf{u}^{n+1} \\ \eta^{n+1} \end{bmatrix} = \begin{bmatrix} \mathbf{R}_u^t \\ \mathbf{R}_\eta^t \end{bmatrix}, \tag{7}$$

where

$$\mathbf{B}^t = \frac{\mathbf{B}}{\Delta t}, \quad \mathbf{R}_u^t = \frac{\mathbf{R}_u}{\Delta t}, \quad \tilde{\mathbf{B}}^t = \frac{\tilde{\mathbf{B}}}{\Delta t \eta_0}, \quad \mathbf{R}_\eta^t = \frac{\mathbf{R}_\eta}{\Delta t \eta_0}. \tag{8}$$

The Helmholtz problem for the geopotential perturbation at each timestep is obtained by solving for the velocity  $\mathbf{u}^{n+1}$  in the above block system to arrive at

$$\mathbf{u}^{n+1} = \mathbf{B}^{-1} (\mathbf{R}_u^t + \Delta t g^{ij} \mathbf{D}^T \eta^{n+1}), \tag{9}$$

and then applying back-substitution to obtain an equation for the geopotential

$$g \tilde{\mathbf{B}} \eta^{n+1} + \Delta t^2 \eta_0 \mathbf{D} g \mathbf{B}^{-1} g^{ij} \mathbf{D}^T \eta^{n+1} = \mathbf{R}'_\eta, \tag{10}$$

where

$$\mathbf{R}'_\eta \equiv g \mathbf{R}_\eta - \Delta t \eta_0 \mathbf{D} g \mathbf{B}^{-1} \mathbf{R}_u. \tag{11}$$

Once the geopotential  $\eta^{n+1}$  is computed, the velocity components  $u^1, u^2$  are computed from (9) where thereafter, shared local nodal values on element boundaries of the velocity components are then averaged.

Furthermore, due to the fact that  $\eta_0, g, \tilde{\mathbf{B}}$  and  $\mathbf{B}^{-1}$  are diagonal, and  $g^{ij}$  can be shown to be symmetric, it is easy to see that the matrix  $\mathbf{H}_{SE}$  is symmetric and positive definite. In effect, an efficient preconditioned conjugate gradient method can be constructed by using local element direct solvers for the Helmholtz problem with zero Neumann pressure gradient boundary conditions. The inverse of each local Helmholtz operator matrix restricted to an element  $\mathbf{H}|_{\Omega^e}$  is computed once and stored for use as a block-Jacobi preconditioner. This preconditioning technique enjoys a computational structure ideal for parallel processors due to the fact that the preconditioner is strictly local to an element and requires no global communication.

### 3.2 The Empirical Backus-Gilbert Reproducing Kernel Discretization

Coupled with the global spectral-element method for use in regional approximation of the shallow-water model, the empirical Backus–Gilbert reproducing kernel discretization method, originally introduced in Blakely [5] has been demonstrated to produce highly accurate solutions to time-dependent nonlinear PDEs while being endowed with great freedom in choosing the approximation space for building the reproducing kernel. Furthermore, as the name of the method suggests, the EBGRK is completely empirical with respect to the distribution of meshless nodes in the domain of interest. For complete details of the method the reader is referred to [5].

The EBGRK method considers a quasi-interpolant of the form

$$Pu(\mathbf{x}) = \sum_{i=1}^N u(\mathbf{x}_i)\Psi_i(\mathbf{x}), \tag{12}$$

where  $\mathbf{u} = [u(\mathbf{x}_1), \dots, u(\mathbf{x}_N)]^T$  represents the given data on a set of  $N$  distinct evaluation nodes  $\mathcal{X} = \{\mathbf{x}_1, \dots, \mathbf{x}_N\}$  on a bounded domain  $\Omega \subset \mathbb{R}^2$ . The finite set of nodes  $\mathcal{X}$  is endowed with a *separation distance* defined as

$$q_{\mathcal{X}} := \frac{1}{2} \min_{\mathbf{x}_j \neq \mathbf{x}_i} \|\mathbf{x}_i - \mathbf{x}_j\|_2.$$

The quasi-interpolant  $\Psi_i(\mathbf{x})$ , or discrete reproducing kernel in some literature, is constructed to be minimized in a discrete quadratic expression subject to some approximation space reproduction constraints. Details on constructing the empirical reproducing kernel is out of the scope of this paper. We refer the reader to Blakely [5] for the construction of the kernel and efficient numerical implementation.

To initiate regional meshless approximation on the cubed-sphere, consider the domain  $\Omega^M = \cup_{i=1}^M \Omega^{e_i}$  constructed of  $M$  contiguous elements on the discretized cubed-sphere. For simplicity, we will assume  $\Omega^M$  lies on only one face of the the cube. Building a meshless approximation space  $\mathcal{V}_{\Psi, \mathcal{X}}$  begins by randomly distributing two sets of  $N_M$  distinct collocation nodes in  $\Omega^M$  and on its boundary  $\partial\Omega^M$  giving two sets  $\mathcal{X}_M^V, \mathcal{X}_M^\eta$  such that  $\mathcal{X}_M^V = \mathcal{X}_M^\eta$ . Using the EBGRK method, the kernels  $\Psi_i(\cdot)$  and  $\Phi_i(\cdot)$  are constructed to form the discrete spaces  $\mathcal{V}_{\Psi, \mathcal{X}} = \text{span}\{\Psi_i(\cdot), i = 1, \dots, N_M\}$  and  $\mathcal{M}_{\Phi, \mathcal{X}} = \text{span}\{\Phi_i(\cdot), i = 1, \dots, N_M\}$  and with respect to the sets  $\mathcal{X}_M^V$  and  $\mathcal{X}_M^\eta$ , respectively.

For writing the cubed-sphere shallow water equations in strong form, we utilize the matrix-vector form of the equations originally given in [21]. As in any other collocation method, we construct the set of Dirac delta test functionals  $\Pi_{\mathcal{X}_M^V} = \{\delta_{\mathbf{x}_1}, \dots, \delta_{\mathbf{x}_{N_M}}\} \subset (H^1)'(\Omega^M)$  and multiply each of the velocity components and geopotential by each Dirac delta test functional  $\delta_{\mathbf{x}_i} \in \Pi_{\mathcal{X}_M^V}$  evaluated which gives

$$\begin{aligned}
 & \langle \delta_{\mathbf{x}_j}, u^{i(n+1)} \rangle + \Delta t \left\langle \delta_{\mathbf{x}_j}, g^{ij} \frac{\partial}{\partial x^j} (\eta)^{n+1} \right\rangle \\
 & = \langle \delta_{\mathbf{x}_j}, u^{i(n-1)} \rangle - \Delta t g^{ij} \left\langle \delta_{\mathbf{x}_j}, \frac{\partial}{\partial x^j} (\eta)^{n-1} \right\rangle + 2\Delta t \langle f_u^{i(n)}, \delta_{\mathbf{x}_j} \rangle, \\
 & \langle \delta_{\mathbf{x}_j}, \eta^{n+1} \rangle + \Delta t \left\langle \delta_{\mathbf{x}_j}, \frac{\eta_0}{g} \frac{\partial}{\partial x^j} (g u^j)^{n+1} \right\rangle \\
 & = \langle \delta_{\mathbf{x}_j}, \eta^{n-1} \rangle - \Delta t \left\langle \delta_{\mathbf{x}_j}, \frac{\eta_0}{g} \frac{\partial}{\partial x^j} (g u^j)^{n+1} \right\rangle + 2\Delta t \langle \delta_{\mathbf{x}_j}, f_\eta^n \rangle \quad (13)
 \end{aligned}$$

with

$$\langle \delta_{\mathbf{x}_j}, f_u^{i(n)} \rangle = -\epsilon_{jk} \langle \delta_{\mathbf{x}_j}, g^{ij} u^{k(n)} g f \rangle - \left\langle \delta_{\mathbf{x}_j}, g^{ij} u_k^n \frac{\partial}{\partial x^j} u^{k(n)} \right\rangle,$$

and

$$\langle \delta_{\mathbf{x}_j}, f_\eta^n \rangle = - \left\langle \delta_{\mathbf{x}_j}, u^j \frac{\partial \eta^n}{\partial x^j} \right\rangle.$$

In order to approximate these equations spatially with the EBG RK method, we look for a solution  $\mathbf{u} \in (\mathcal{V}_{\Psi, \mathcal{X}})^2 \subset (H^1(\Omega^M))^2$  and  $\eta \in \mathcal{V}_{\Psi, \mathcal{X}}$  by taking for all  $n \geq 0$

$$u_k^n(\mathbf{x}_j) = \sum_{i=1}^{N_M} \tilde{u}_k^n(\mathbf{x}_i) \Psi_i(\mathbf{x}_j), \quad \eta^n(\mathbf{x}_j) = \sum_{i=1}^{N_M} \tilde{\eta}^n(\mathbf{x}_i) \Phi_i(\mathbf{x}_j) \quad \text{for } \mathbf{x}_k \in \mathcal{X}_M^V,$$

where  $\tilde{u}_k^n(\mathbf{x}_i)$  and  $\tilde{\eta}^n(\mathbf{x}_i)$  are the approximated values at the collocation nodes  $\mathbf{x}_i$  at time step  $n$ . Substituting these into (13) and applying the Dirac delta functionals, we get for all  $\delta_{\mathbf{x}_j} \in \Pi_{\mathcal{X}_M^V}$

$$\begin{aligned}
 & \left\langle \delta_{\mathbf{x}_j}, \sum_{i=1}^{N_M} \tilde{u}^{k(n+1)}(\mathbf{x}_i) \Psi_i(\mathbf{x}) \right\rangle + \left\langle \Delta t g^{ij} \frac{\partial}{\partial x^j} \delta_{\mathbf{x}_j}, \sum_{i=1}^{N_M} \tilde{\eta}^{n+1}(\mathbf{x}_i) \Phi_i(\mathbf{x}) \right\rangle \\
 & = \left\langle \delta_{\mathbf{x}_j}, \sum_{i=1}^{N_M} \tilde{u}^{k(n-1)}(\mathbf{x}_i) \Psi_i(\mathbf{x}) \right\rangle + \left\langle \Delta t g^{ij} \frac{\partial}{\partial x^j} \delta_{\mathbf{x}_j}, \sum_{i=1}^{N_M} \tilde{\eta}^{n-1}(\mathbf{x}_i) \Phi_i(\mathbf{x}) \right\rangle \\
 & \quad + \langle 2\Delta t \delta_{\mathbf{x}_j}, f_u^{i(n)} \rangle, \\
 & \left\langle \delta_{\mathbf{x}_j}, \sum_{i=1}^{N_M} \tilde{\eta}^{n+1} \Phi_i(\mathbf{x}) \right\rangle + \left\langle \Delta t \frac{\eta_0}{g} \frac{\partial}{\partial x^j} \delta_{\mathbf{x}_j}, g \sum_{i=1}^{N_M} \tilde{u}^{j(n+1)}(\mathbf{x}_i) \Psi_i(\mathbf{x}) \right\rangle \\
 & = \left\langle \delta_{\mathbf{x}_j}, \sum_{i=1}^{N_M} \tilde{\eta}^{n-1}(\mathbf{x}) \Phi_i(\mathbf{x}) \right\rangle - \left\langle \Delta t \frac{\eta_0}{g} \frac{\partial}{\partial x^j} \delta_{\mathbf{x}_j}, g \sum_{i=1}^{N_M} \tilde{u}^{j(n-1)}(\mathbf{x}_i) \Psi_i(\mathbf{x}) \right\rangle \\
 & \quad + 2\langle \Delta t \delta_{\mathbf{x}_j}, f_\eta^n \rangle. \quad (14)
 \end{aligned}$$

The calculation of

$$g_{\mathbf{x}_j} \frac{\partial \Psi_i(\mathbf{x}_j)}{\partial x^k}, \quad \mathbf{x}_j \in \mathcal{X}_M^V,$$

which is used in the divergence terms of the strong form shallow water system is made prior to time stepping and stored as matrices in the form

$$D_k = \begin{pmatrix} g_{\mathbf{x}_1} \Upsilon_1(\mathbf{x}_1) & g_{\mathbf{x}_1} \Upsilon_2(\mathbf{x}_1) & \cdots & g_{\mathbf{x}_1} \Upsilon_{N_M}(\mathbf{x}_1) \\ g_{\mathbf{x}_2} \Upsilon_1(\mathbf{x}_2) & g_{\mathbf{x}_2} \Upsilon_2(\mathbf{x}_2) & \cdots & g_{\mathbf{x}_2} \Upsilon_{N_M}(\mathbf{x}_2) \\ \vdots & & & \\ g_{\mathbf{x}_{N_M}} \Upsilon_1(\mathbf{x}_{N_M}) & g_{\mathbf{x}_{N_M}} \Upsilon_2(\mathbf{x}_{N_M}) & \cdots & g_{\mathbf{x}_{N_M}} \Upsilon_{N_M}(\mathbf{x}_{N_M}) \end{pmatrix}, \quad (15)$$

where  $\Upsilon_j(\cdot)$  denotes the differential operator  $\frac{\partial}{\partial x^k}$  acting on the kernel  $\Psi_j(\cdot)$ , which was shown how to be constructed in Section 3.2. A similar matrix  $g_{ij} D_k^T$  used in calculating the gradient of the geopotential in strong form is also computed and stored prior to time stepping. These matrices are akin to the two-dimensional derivative matrix  $\mathbf{D}_i$  of size  $N^2 \times N^2$  in the spectral element formulation.

Using notation borrowed from the spectral element formulation, we write the discretized equations in matrix form with  $\mathbf{D} = (D_1, D_2)$  as the derivative matrices with respect to the collocation nodes and  $\mathbf{B}, \tilde{\mathbf{B}}$  as the collocation matrices for the velocity and geopotential, respectively. This leads to the system

$$\begin{bmatrix} \mathbf{B}^t & -\mathbf{D}^t \\ \mathbf{D}^t & \tilde{\mathbf{B}}^t \end{bmatrix} \begin{bmatrix} \tilde{\mathbf{u}}^{n+1} \\ \tilde{\eta}^{n+1} \end{bmatrix} = \begin{bmatrix} \mathbf{R}_u^t \\ R_\eta^t \end{bmatrix},$$

where

$$\mathbf{B}^t = \frac{\mathbf{B}}{\Delta t}, \quad \mathbf{R}_u^t = \frac{\mathbf{R}_u^t}{\Delta t}, \quad (16)$$

$$\tilde{\mathbf{B}}^t = \frac{\tilde{\mathbf{B}}}{\Delta t \eta_0}, \quad R_\eta^t = \frac{R_\eta}{\Delta t \eta_0}. \quad (17)$$

Performing the Uzawa velocity-geopotential decoupling algorithm where we solve for the velocity  $\mathbf{u}^{n+1}$  in the above block system to arrive at

$$\tilde{\mathbf{u}}^{n+1} = \mathbf{B}^{-1}(\mathbf{R}_u^t + \Delta t g^{ij} \mathbf{D}^T \tilde{\eta}^{n+1}), \quad (18)$$

and then applying back-substitution to obtain an equation for the geopotential at the time step  $n + 1$ .

$$g \tilde{\mathbf{B}} \tilde{\eta}^{n+1} + \Delta t^2 \eta_0 \mathbf{D} g \mathbf{B}^{-1} g^{ij} \mathbf{D}^T \tilde{\eta}^{n+1} = R_\eta', \quad (19)$$

where

$$R_\eta' \equiv g R_\eta - \Delta t \eta_0 \mathbf{D} g \mathbf{B}^{-1} \mathbf{R}_u.$$

As with the spectral element case, we are now concerned with the solution to the Helmholtz problem for the geopotential. Although the meshless collocation method yields a strong form of the discrete shallow water model, the resulting discrete Helmholtz equation is similar to the spectral element Helmholtz equation in that the matrix operator

$$H_{MM} = g\tilde{B} + \Delta t^2 \eta_0 \mathbf{D}g\mathbf{B}^{-1}g^{ij}\mathbf{D}^T \tag{20}$$

is symmetric and positive definite and of size  $N_M \times N_M$ . It is important to notice that the term

$$\mathbf{D}g\mathbf{B}^{-1}g^{ij}\mathbf{D}^T$$

is a discrete pseudo-Laplacian operator on  $\Omega^M$ , a local domain on the sphere  $S^2$ . Because of the fact that the domain is locally defined on the sphere, essential boundary conditions on  $\partial\Omega^M$  are needed in order to show direct equivalence to a local Helmholtz elliptic problem on  $\Omega^M$ . This was not the case with the spectral element discretization on the sphere since no boundary conditions are needed for the global shallow water model. As a result, the boundary information on  $\partial\Omega^M$  must come from the spectral element approximation in order to produce a unique solution to the discrete Helmholtz problem (19). As we propose in the next section, if  $\tilde{\eta}^{n+1}$  is the unique solution to this local Helmholtz problem at time  $n + 1$  with respect to the boundary information given by a global spectral element discretization at time  $n + 1$ , then  $\tilde{\eta}^{n+1}$  is an approximation to the geopotential field restricted to  $\Omega^M$  at time step  $n + 1$ . To accomplish this task, we adapt the three-field domain decomposition algorithm developed in [7] for coupling the two Helmholtz discretizations, which is discussed in the next section.

#### 4 Coupling the Meshless and SE Approximations

Because the meshless approximation is done locally utilizing the strong formulation of the shallow-water equations on a local domain  $\Omega^M$ , certain transition conditions are needed on the boundary of the subdomain connecting the meshless and spectral-element approximations in order to satisfy continuity and flux conditions of the solution along with the artificial fluxes of the field variables. In 1994, Brezzi and Marini (see [7]) developed a method termed the *three-field formulation* for *hybrid* finite-element formulations where the goal was to give the possibility of coupling different finite-element approximations using different meshes and basis functions from one subdomain to another.

In this paper, we extend the idea of the three-field technique to couple spectral-element and meshless collocation methods. As shown in the previous sections, the manner in which we couple the two approximation schemes is done implicitly. Namely, after deriving the semi-implicit method, a symmetric positive definite discrete Helmholtz type equation was left to be solved at each time step for the geopotential. With the solution of the geopotential at hand, it could then be used to

approximate the velocity field at the same time step. So the question that remains is how to solve Helmholtz equations for the coupled meshless/spectral-element approximation. In this section we consider solving the elliptic problem

$$Hu = \Delta u(\mathbf{x}) + g(\mathbf{x})u(\mathbf{x}) = f(\mathbf{x}), \quad \in S^2, \quad (21)$$

where  $S^2$  is the unit sphere which is discretized via the cubed-sphere method discussed in Section 2. The fact that spatial discretization is not performed with spherical harmonics but rather on a cubed-sphere mesh allows for an adaptive localized approximation using meshless collocation via domain decomposition. Thus the heart of the hybrid shallow water model lies in the efficient handling of the Helmholtz equation on the sphere using the meshless/spectral-element formulation.

For proper stability analysis of this new three-field formulation for coupling spectral-elements and meshless collocation including Babuška–Brezzi inf-sup type conditions, the reader is referred to the paper by Blakely [6]. In order to introduce the method, we must first discuss the necessary approximation spaces that will be used in the formulation and discretization and their relevant physical meaning.

#### 4.1 The Continuous Three-Field Formulation

Using the notation from the previous subsections, suppose we have are given a subdomain of  $M$  unioned elements  $\Omega^M = \cup_{i=1}^M \Omega^{e_i}$ . For simplicity of exposition of the three-field method, we assume  $\Omega^M$  is on one face of the cube. Let  $\Gamma_{SE/M}$  denote the boundary of  $\Omega^M$  which we will call the *interface* of the hybrid method between the spectral element and meshless collocation approximations. Finally, we denote  $\Omega^{SE} = \Omega - \Omega^M$ , namely the collection of spectral elements not in  $\Omega^M$  and then set  $\Omega_1 := \Omega^{SE}$ ,  $\Omega_2 := \Omega^M$  and  $\Gamma_i := \partial\Omega_i$ , for  $i = [1, 2]$ , which are the boundaries of these domains sharing the interface  $\Gamma_{SE/M}$ .

In addition to the Sobolev space  $H_0^1(\Omega_i)$  on each domain  $\Omega_i$ , utilizing the interface  $\Gamma_{SE/M}$  leads to two additional types of spaces that will be needed for domain decomposition. We define a trace space and two dual spaces on  $\Gamma_{SE/M}$  by considering  $H^{1/2}(\Gamma_{SE/M})$  with corresponding norm  $\|\cdot\|_\Gamma := \|\cdot\|_{H^{1/2}(\Gamma_{SE/M})}$  and denote the dual of this space as  $H^{-1/2}(\Gamma)$ . Furthermore we introduce two spaces of Lagrangian multipliers which provide the role of enforcing necessary boundary continuity over the interface  $\Gamma_{SE/M}$  and are defined as  $\Lambda_i := H^{-1/2}(\Gamma_i)$  for  $i = [1, 2]$  which can be regarded as the dual of the trace spaces associated with the two Hilbert spaces  $H^1(\Omega_1)$  and  $H^1(\Omega_2)$ . The Lagrangian multiplier space is endowed with the standard scalar inner product  $L^2(\Gamma)$ ,  $\langle \Lambda^i, H^{1/2} \rangle_\Gamma = \int_\Gamma \lambda_i u^i ds$  for  $u^i \in H^1(\Omega)$ . The third function space which acts as the global continuity space for the hybrid approximation is defined on the interface  $\Gamma$  as restrictions of functions on the sphere  $S^2$  to the interface. Namely

$$\Phi := \{v \in L^2(\Gamma) : \exists u \in H^1(S^2), u = v \text{ on } \Gamma\}. \quad (22)$$

Global norms for the spaces  $V_i := H_0^1(\Omega_i)$  and  $\Lambda_i$  can be given as broken norms over  $\Omega_i$

$$\|\mathbf{u}\|_V := \left( \sum_{i=1}^2 \|u^i\|_{1,\Omega_i}^2 \right), \quad \|\lambda\|_\Gamma := \left( \sum_{i=1}^2 \|\lambda^i\|_{H^{-\frac{1}{2}}(\Gamma_i)}^2 \right),$$

and can easily be shown to be Hilbert spaces with these induced norms. Furthermore, with the use of extension operators, the interface continuity space is endowed with the norm

$$\|\varphi\|_\Phi := \inf_{u|_{\Gamma}=\varphi} \|u\|_{1,\Omega}.$$

With the three approximation spaces at hand, the three-field formulation of the Helmholtz problem can be written for the two subdomains utilizing the additional two interface spaces  $\Lambda_i$  and the global continuity space  $\Phi$ . Using the dual product notation  $\langle \cdot, \cdot \rangle_i = \langle H^{-1/2}(\Gamma_i), H^{1/2}(\Gamma_i) \rangle$  the following variational form is called the three-field formulation. Find  $\mathbf{u} \in \mathbf{V}$ ,  $\lambda \in \Lambda$ , and  $\varphi \in \Phi$  such that

$$\left\{ \begin{array}{l} \text{(i)} \quad \sum_{i=1}^2 (a_{\Omega_i}(u^i, v^i) - \langle \lambda^i, v^i \rangle_{\Gamma_i}) = \sum_{i=1}^2 (f, v^i)_{\Omega_i}, \quad \forall \mathbf{v} \in \mathbf{V}, \\ \text{(ii)} \quad \sum_{i=1}^2 \langle \mu^i, u^i - \varphi \rangle_{\Gamma_i} = \mathbf{0}, \quad \forall \mu \in \Lambda \\ \text{(iii)} \quad \sum_{i=1}^2 \langle \lambda^i, \psi \rangle_{\Gamma_i} = \mathbf{0}, \quad \forall \psi \in \Phi \end{array} \right. \quad (23)$$

The bilinear operator  $a_{\Omega_i}$  stems from the weak formulation of the Helmholtz equation and is defined as

$$a_{\Omega_i}(u^i, v^i) = \int_{\Omega_i} \nabla u^i \nabla v^i + g u^i v^i d\Omega_i.$$

Furthermore, the inner products of the form

$$\langle H^{-1/2}(\Gamma_i), H^{1/2}(\Gamma_i) \rangle_{\Gamma_i}$$

signify the artificial boundary or interface matching conditions. To be more specific, the second equation enforces weak continuity along the interface  $\Gamma_i$  with the solution  $u^i$  on  $\Omega_i$  with respect to the interface continuity variable  $\varphi$ . The third equation serves two purposes: (1) it further constrains the space of Lagrangian multipliers  $\Lambda$  by adding orthogonality conditions with the interface space  $\Phi$ , and (2) it renders the discrete formulation of the above system as a symmetric positive definite system

which can then be solved for the global solution  $(\mathbf{u}, \lambda, \varphi)$  using a preconditioned conjugate gradient method as will be shown in the next subsection.

We first note that a key observation in the three-field formulation comes from the first two equations of (23). For a given  $\varphi$  on the skeleton  $\Gamma$ , the first two equations are local Dirichlet problems where the boundary conditions on  $\Gamma_i$  are imposed in the weak sense. Because of this, one can show that the local problems are well-posed for a given sufficient  $\varphi$ . For a complete analysis of the three field method for coupling meshless and spectral-element approximations for elliptic equations, the reader is referred to the paper by Blakely [6]. The thesis by Rabin [16] and relevant references therein also give much insight to the three-field variational formulation in the finite-element context.

## 4.2 Discrete Version of the Three-Field Formulation

The difficulty in passing to the discrete formulation the variational problem (23) is in choosing the appropriate discrete subspaces of  $\mathbf{V}$ ,  $\Lambda$ , and  $\Phi$ . Arbitrarily choosing the subspaces can lead to unstable solutions of the discrete variational problem primarily due to not satisfying the discrete versions of the inf-sup conditions, so careful consideration of the spaces is necessary. In past approaches to the method, usually the discretization of the space  $\mathbf{V}$  is chosen first and then  $\Lambda$  and  $\Phi$  are chosen thereafter to satisfy the inf-sup requirements. In this section, we propose a discrete approximation to the three-fields formulation by considering the spectral-element and meshless collocation methods as the discretization tools which will then lead to the hybrid meshless/spectral-element method for the shallow water equations on the sphere.

With  $\Omega_1$  defining the domain for the spectral element approximation and the regional domain  $\Omega_2$  being allocated for meshless collocation, we define the space  $V_N^1 := \mathbb{P}_{N,N_e} \cap H^1(\Omega_1)$ , where  $\mathbb{P}_{N,N_e}$  is the space of piecewise continuous functions that map to polynomials of degree less than or equal  $N$  to the reference element  $\Omega^e$ . Namely,

$$\mathbb{P}_{N,E}(\Omega_1) := \{v(\mathbf{x}^e(\mathbf{r}))|_{\Omega^e} \in \mathbb{P}_N(r) \otimes \mathbb{P}_N(s), e = 1, \dots, N_e \text{ such that } \Omega^e \in \Omega_1\},$$

where  $\mathbb{P}_N(r)$  is the space of all polynomials of degree less than or equal to  $N$ . To restrict this space to  $\Omega_1$ , we include all  $\Omega^e$  such that  $\Omega_1 \cap \Omega^e \neq \emptyset$ . This approximation space will provide each component of the velocity field on the spectral element partition  $\Omega_1$ . As described in Section 3.1, the discrete geopotential space is obtained by utilizing the staggered grid approach and setting  $M_N^1 := \mathbb{P}_{N-2,N_e} \cap H^1(\Omega_1)$ . Since the boundaries on each element  $\Omega^e$  are essential to the three-field method, the  $N - 2$  Gauss–Lobatto–Legendre distribution of nodes is used for the geopotential grid, which is contrary to many spectral element staggered grids which use Gauss–Legendre nodes for the geopotential/pressure field.

The regional domain  $\Omega_2$  allocates a collocation approximation by considering a random (or uniform) distribution of  $N_M$  distinct collocation nodes  $\Omega^M$  and on its

boundary  $\partial\Omega^M$  giving two sets  $\mathcal{X}_M^V, \mathcal{X}_M^\eta$  such that  $\mathcal{X}_M^V = \mathcal{X}_M^\eta$ . We then construct the approximation space  $M_{NM}^2 = V_{NM}^2 := \text{span}\{\Psi_1(\mathbf{x}), \dots, \Psi_{NM}(\mathbf{x})\}$  as defined in Section 3.2.

With the spaces defined for the velocity and geopotential fields on each subdomain  $\Omega_i$ , the Lagrangian multiplier spaces  $\Lambda^i$  for the interface boundaries  $\Gamma_i$  can now be constructed by using the spaces  $M_N^1$  and  $M_{NM}^2$ . Since  $M_N^1$  defines a spectral approximation of order  $N - 2$ , we define the Lagrangian multiplier space for  $\Gamma_1$  as the space of Lagrangian interpolants of order less than or equal to  $N$  and restricted to  $\Gamma_1$ . This is given by

$$\begin{aligned} \Lambda_N^1 &= \mathbb{P}_{N,E}(\Gamma_1) \\ &:= \{ \lambda(\mathbf{x}^e(r))|_{\Omega^e} \in \mathbb{P}_{N-4}(r)|_{\Gamma_1}, e = 1, \dots, N_e \text{ such that } \Omega^e \cap \Gamma_1 \neq \emptyset \}. \end{aligned} \tag{24}$$

Using such a space for  $H^{-\frac{1}{2}}(\Gamma_1)$ , it can be shown that the discrete inf-sup condition for the interface inner product on  $\Gamma_1$  is satisfied. Namely, for some constant  $C_{1,N}$  dependent on the degree  $N$  of the spectral elements, we have

$$\inf_{\lambda_N^1 \in \Lambda_N^1 / \{0\}} \sup_{\eta_N^1 \in M_N^1 / \{0\}} \frac{\langle B\lambda_N^1, \eta_N^1 \rangle_{\Gamma_1}}{\|\eta_N^1\|_{M_{NM}^1} \|\lambda_N^1\|_{\Lambda_N^1}} = \frac{\langle \lambda_N^1, \eta_N^1 \rangle_1}{\|\eta_N^1\|_{M_{NM}^1} \|\lambda_N^1\|_{\Lambda_N^1}} > C_{1,N}$$

is satisfied. This result is proved in the paper on the Mortar Spectral Element method by Ben Belgacem et al. [3] in a similar interface inner product using Lagrangian multipliers.

In order to complete the space  $\Lambda$  we need the additional interface space on  $\Omega_2$ . On the boundary  $\Gamma_2$ , a second meshless collocation space for  $\Lambda_N^2$  is constructed using a random distribution of  $N_{M_\Gamma}$  nodes restricted to the interface  $\Gamma_2$  producing the set  $X_{\Gamma_2}$ . Using the EBGRK method presented in Section 3.2, the Lagrangian multiplier space for  $\Gamma_2$  is taken to be  $\Lambda_{NM}^2 = \text{span}\{\Psi_1^\lambda(\mathbf{x}), \dots, \Psi_{NM}^\lambda(\mathbf{x}) : \mathbf{x} \in \Gamma_2\} \subset H^{-1/2}(\Gamma_2)$  where  $\Psi_i^\lambda(\cdot)$  denotes the  $i$ -th discrete reproducing kernel function on  $X_{\Gamma_2}$ .

Lastly, in order to connect the two pairs of approximation spaces  $(M_N^1, \Lambda_N^1)$  and  $(M_{NM}^2, \Lambda_{NM}^2)$  on  $\Omega_1$  and  $\Omega_2$ , respectively, we build a suitable discrete subspace of  $\Phi$  by taking the Lagrangian interpolants constructed from Legendre polynomials of degree  $N - 2$  restricted to  $\Gamma$ . Namely,

$$\Phi_N := \{ \varphi(\mathbf{x}^e(r))|_{\Omega^e} \in \mathbb{P}_{N-2}(r)|_\Gamma, e = 1, \dots, N_e, \text{ such that } \Omega^e \cap \partial\Omega \neq \emptyset \}.$$

This will ensure that the discrete inf-sup condition for  $\Phi$  and  $\Lambda_N^1$  on  $\Gamma_1$  is satisfied.

The last issue we need to resolve in this three field formulation is complying with the strong form of the shallow water equations on  $\Omega_2$ . To this end, since  $\Omega_2$  utilizes a meshless collocation technique, we define the set of test distributions on  $\Omega_2$  as  $M_{\delta,NM}^2 = \{ \delta_{\mathbf{x}_i} : \mathbf{x}_i \in X_\eta^{NM} \}$  where  $\delta_{\mathbf{x}_i}$  is the Dirac delta function at node  $\mathbf{x}_i$ .

The original variational formulation in (23) can now be modified as follows. Find  $(\eta_N^1, \lambda_N^1, \eta_N^2, \lambda_N^2, \varphi) \in M_N^1 \otimes \Lambda_N^1 \otimes M_{NM}^2 \otimes \Lambda_{NM}^2 \otimes \Phi$  such that

$$\left\{ \begin{array}{l} \text{(i)} \quad a_{\Omega_1}(\eta_N^1, \chi_N^1) - \langle \lambda_N^1, \chi_N^1 \rangle_{\Gamma_1} = (f, \chi_N^1)_{\Omega_1}, \quad \forall \chi_N^1 \in M_N^1, \\ \text{(ii)} \quad \langle \mu_N^1, \eta_N^1 - \varphi_N \rangle_{\Gamma_1} = \mathbf{0}, \quad \forall \mu_N^1 \in \Lambda_N^1, \\ \text{(iii)} \quad \langle \lambda_N^1, \psi_N \rangle_{\Gamma_1} = \mathbf{0}, \quad \forall \psi_N \in \Phi, \end{array} \right. \quad (25)$$

and

$$\left\{ \begin{array}{l} \text{(i)} \quad a_{\Omega_2}(\eta_N^2, \chi_N^2) - \langle \lambda_N^2, \chi_N^2 \rangle_{\Gamma_2} = (f, \chi_N^2)_{\Omega_2}, \quad \forall \chi_N^2 \in M_{\delta, NM}^2, \\ \text{(ii)} \quad \langle \mu_N^2, \eta_N^2 - \varphi_N \rangle_{\Gamma_2} = \mathbf{0}, \quad \forall \mu_N^2 \in \Lambda_{NM}^2, \\ \text{(iii)} \quad \langle \lambda_N^2, \psi_N \rangle_{\Gamma_1} = \mathbf{0} \quad \forall \psi_N \in \Phi. \end{array} \right. \quad (26)$$

Once the discrete approximation spaces have been chosen and numerical integration has been done, an efficient manner in solving this is to construct the Schur compliment system and then apply a conjugate gradient method. To do this, we first write (25) and (26) in algebraic form as:

$$\begin{aligned} A_i \eta_i - B_i^T \lambda_i &= \mathbf{f}_i, \\ -B_i \eta_i + C_i^T \varphi &= \mathbf{0}, \\ C_i \lambda_i &= \mathbf{0}, \end{aligned}$$

for  $i = 1, 2$ . Now applying block Gaussian elimination to the linear system, we obtain a linear system for  $\varphi$  as

$$\mathcal{S} \varphi = \mathbf{g}, \quad (27)$$

where  $\mathcal{S} = \mathcal{S}_1 + \mathcal{S}_2$ ,  $\mathbf{g} = \mathbf{g}_1 + \mathbf{g}_2$  and

$$\mathcal{S}_i := C_i D_i^{-1} C_i^T, \quad \mathbf{g}_i := C_i D_i^{-1} B_i A_i^{-1} \mathbf{f}_i, \quad D_i := B_i A_i^{-1} B_i^T, \quad i = 1, 2. \quad (28)$$

The  $\mathcal{S}$  matrix can be considered as the Schur compliment matrix with respect to  $\mathbf{u}$  and  $\lambda$  of the entire system defined above. Furthermore, it was shown by Brezzi in [7] that the Schur compliment  $\mathcal{S}$  is symmetric and positive definite if the matrices  $B_i^T$  and  $C_i$  have full rank. One can then apply a conjugate gradient method to the system (27) to obtain the solution of the elliptic problem on the global domain. It can be remarked that by definition of  $\mathbf{g}_i$ , the calculation of a conjugate gradient iteration requires the solution to the local Helmholtz equation in each subdomain  $\Omega_i$ ,  $i = 1, 2$ . Block-Jacobi preconditioning is used to solve each of these local Helmholtz problems by considering zero Neumann conditions for each local problem. This way, each local

Helmholtz problem has a unique solution and in effect, the matrix  $A_i$  has an inverse which can be calculated before time-stepping.

The last issue of the discrete three-field formulation is related to the efficient construction of the matrices  $C$  and  $B$ . As they include the integration of the basis functions for the Lagrangian multiplier spaces and the interface space and are independent of the data, they can be calculated and stored prior to time stepping as well. The matrices have the form

$$\mathbf{C}_i(j, k) = \langle \mu_{i,j}, \phi_k \rangle_{\Gamma}, \quad \mu_{i,j} \in \Lambda_N^i, \quad \phi_{i,k} \in \Phi^N, \quad (29)$$

$$\mathbf{B}_i(j, k) = \langle \eta_{i,j}, \mu_{i,k} \rangle_{\Gamma_i}, \quad \mu_{i,j} \in \Lambda_N^i, \quad \eta_{i,k} \in M_N^i. \quad (30)$$

For  $i = 2$ , the above calculations involve integration on a spectral grid using meshless reproducing kernels. The choice of the  $\beta$  parameter and  $N_M$  for a given radial basis that constructs the reproducing kernel determines the stability of the entire hybrid model. A study on these parameters is given in full detail in Blakely [6].

## 5 Numerical Experiments

As is it well established that the spherical rotational shallow-water equations represent a simplified model of the dynamica of the atmosphere, Williamson et al. [22] have proposed a series of eight test cases for the equations in spherical geometry. It is proposed by the authors that in order to have any type of success with a new numerical scheme for an a climate model, successful integrations of the numerical scheme with these test cases are imperative. The purpose of the tests are to examen the sensitivites of a numerical scheme with many computational challenges faced in atmospheric modeling such as stabilization of the scheme for large time steps over a long period of time, the pole problem, simulating flows which have discontinuous first-derivatives in the potential vorticity, and simulating flows over mountain topographies.

### 5.1 Test Case 2: Global Steady State Nonlinear Zonal Geostrophic Flow

As the second test case, a steady state flow to the full non-linear shallow water equations is prescribed and the challenge for a numerical scheme is simply to test its numerical stability with respect to  $l_1$ ,  $l_{inf}$  errors over time. Since the flow is steady, the numerical scheme should be able to integrate the model for many steps without the addition any filtering. The velocity field is given as

$$u = u_0(\cos \theta \cos \alpha + \cos \lambda \sin \theta \sin \alpha),$$

$$v = -u_0 \sin \lambda \sin \alpha,$$

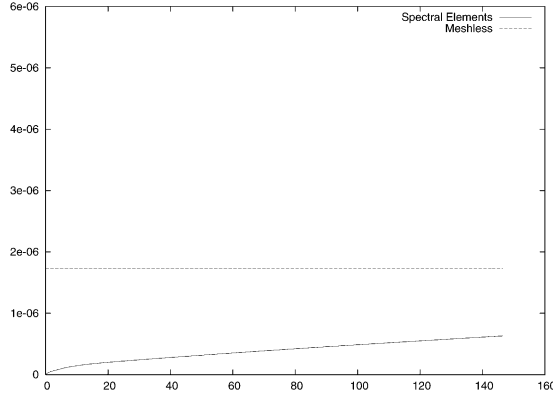


**Fig. 2.** Plot of  $l_1$  errors of the spectral element and meshless geopotential solutions on face 2 of the cubed sphere using 256 (64 per element) nodes for the evaluation of the solutions.

which is non-divergent. The analytic geopotential field is given by

$$\eta = gh_0 - \left( a\Omega u_0 + \frac{u_0^2}{2} \right) (-\cos \lambda \cos \theta \sin \alpha + \sin \theta \cos \alpha)^2,$$

with constants  $u_0 = 2\pi a / (12 \text{ days})$  and  $gh_0 = 2.94 \times 10^4 \text{ m}^2/\text{s}^2$ .

For this numerical experiment, we began with 24 total spectral elements (4 on each face) and ran the model for 121 days without any additional filtering. A second integration was performed using on face number 2 of the cube the meshless collocation approximation built from compactly supported radial functions (see [18]). Figure 2 shows the  $l_1$  errors over time of the geopotential solution on face 2 for both the spectral element and meshless collocation approximations.

Notice how errors in the meshless approximation do not grow nearly as fast as in the spectral element approximation, despite not being as accurate. This is due to the collocation properties of the radial basis used. For the geopotential grid, a total 256 Gaussian–Lobatto–Legendre nodes (64 per element) were used at each time step. Furthermore, to obtain an accurate error comparison between the methods, the collocation approximation was evaluated at the spectral element nodes. Similar results for the  $l_{\text{inf}}$  error were also obtained.

### 5.2 Test Case 6: Rossby-Haurwitz Waves

The most interesting of the test cases features an initial condition for the velocity which is actually the analytical solution to the non divergent nonlinear Barotropic equation on the sphere, given as a vorticity equation. We refer the reader to [22] for the initial conditions of the velocity components and geopotential field.

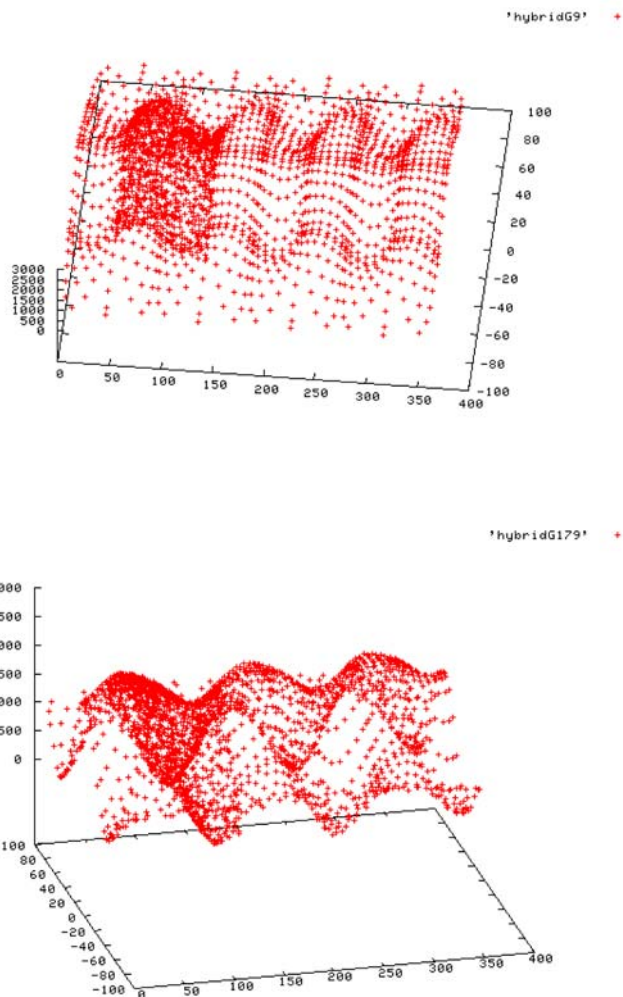


**Fig. 3.** Plots of geopotential approximation using 20 spectral elements and 4 elements allocated to meshless collocation. Plot after 10 and 60 days.

As originally proposed, these waves were expected to evolve nearly steadily with wavenumber 4. However, Thuburn and Li showed that this case is actually weakly unstable in that it will eventually break down once perturbed. This usually occurs after about 40 days depending on the model and parameters used. Figure 3 shows the geopotential layed out on rectangular coordinates for easier viewing. The figure to the left shows the field after 10 days at an angle where the hybrid mesh structure on

the cubed-sphere can easily be seen. Notice that the continuity along the interfaces between the meshless and spectral-element approximations are preserved, meaning the inf-sup conditions along the interface are satisfied.

## 6 Conclusion

In this article, we proposed and developed a new hybrid numerical scheme for the shallow water equations on the sphere based on the merging of several numerical tools including meshless collocation, spectral elements, and the three-field variational formulation. Furthermore, a high-performance Fortran 90 software suite has been developed for the hybrid method for use on distributed memory parallel processors with the message passing interface. Such a successful high-performance implementation ultimately required the use of other Fortran 90 numerical packages for almost half of the computational tasks in the model, such as the domain decomposition. Although much work still remains with theoretical issues of the hybrid approximation scheme such as stability and convergence, the numerical examples in the previous section have clearly shown the method's robustness in approximating the global solution with spectral elements along with localized regions using meshless collocation.

## Acknowledgments

The author would like to thank Franco Brezzi for many fruitful discussions about the three-field method implementation and stability results, and for proof-reading much of the paper. I would also like to thank my advisors, Professors John Osborn and Ferdinand Baer for aiding me in the theoretical issues behind the shallow-water equations and mixed/hybrid methods.

## References

1. F. Baer, H. Wang, J.J. Tribbia and A. Fournier, *Climate Modeling with Spectral Elements*, in progress, 2005.
2. I. Babuška, The finite element method with Lagrangian multipliers. *Numerische Mathematik*, 20:179–192, 1973.
3. F. Ben Belgacem, C. Bernardi, N. Chorfi and Y. Maday, Inf-Sup conditions for the mortar spectral element discretization of the Stokes problem. *Numerische Mathematik*, 85(2):257–281, 2000.
4. S. Bertoluzza, Analysis of a stabilized three-fields domain decomposition method. *Numerische Mathematik*, 93:611–634, 2003.
5. C. Blakely, A new Backus–Gilbert meshless method for initial-boundary value problems. *International Journal on Computational Methods*, to appear, 2006.

6. C. Blakely, A hybrid meshless/spectral-element approximation method for elliptic partial differential equations. *International Journal on Computer Mathematics*, submitted, 2006.
7. F. Brezzi and L.D. Marini, A three-field domain decomposition method. In: A. Quarteroni et al. (Eds), *Decomposition Methods in Science and Engineering*, 1994, pp. 27-34.
8. F. Brezzi and L.D. Marini, The three-field formulation for elasticity problems. *GAMM Mitteilungen*, 38:124–153, 2005.
9. M.D. Buhmann, *Radial Basis Functions: Theory and Implementations*. Cambridge University Press, Cambridge, 2003.
10. G.E. Fasshauer, Matrix-free multilevel moving least-squares methods. In: *Approximation Theory*, X St. Louis, MO, 2002, pp. 271–278.
11. A. Fournier, M.A. Taylor and J.J. Tribbia, The spectral-element atmosphere model: High-resolution parallel computation and localized resolution of regional dynamics. *Monthly Weather Review*, 123:726–748, 2004.
12. J. Galewsky, L.M. Polvani and R.K. Scott, An initial-value problem to test numerical models of the shallow water equations. *Monthly Weather Review*, 2003.
13. A. Gelb and E. Tadmor, Adaptive edge detectors for piecewise smooth data based on the minmod limiter, CSCAMM Report CS-05-06, 2005.
14. E. Kalnay, *Atmopheric Modeling, Data Assimilation and Predictability*. Cambridge University Press, 2003.
15. G.E. Karniadakis and S.J. Sherwin, *Spectral/hp Element Methods for Computational Fluid Dynamics*. Oxford University Press, 1999, 404 pp.
16. G. Rapin, The three-field formulation for elliptic equations: stabilization and decoupling strategies. PhD Thesis, Universität Göttingen, 2003.
17. R. Sadourny, Conservative finite-difference approximations of the primitive equations on quasi-uniform spherical grids. *Monthly Weather Review*, 100:136–144, 1972.
18. R. Schaback, Convergence of unsymmetric kernel based meshless collocation methods. Preprint from <http://www.num.math.uni-goettingen.de/schaback/research/group.html>, 2005.
19. M. Taylor, J. Tribbia and M. Iskandarani, Performance of a spectral-element atmospheric model on the HP Exemplar SPP2000. NCAR Tech. Rep TN-439 + EDD, 16 pp.
20. S.J. Thomas and R.D. Loft, Semi-implicit spectral element atmospheric model. *Journal of Scientific Computing*, 17:339–350, 2002.
21. M. Taylor, J. Tribbia and M. Iskandarani, The spectral element method for the shallow water equations on the sphere. *Journal of Computational Physics*, 130:92–108, 1997.
22. D.L. Williamson, J.B. Drake, J.J. Hack, R. Jakob and P.N. Swarztrauber, A standard test set for numerical approximations to the shallow water equations in spherical geometry. *Journal of Computational Physics*, 102:211–224, 1992.